(FIRST PAGE OF ARTICLE – *align this to the top of page – leave space blank above ABSTRACT*)

ABSTRACT

In the role of structural health monitoring (SHM), Acoustic Emission (AE) analysis is being investigated as an effective method for tracking damage development in large composite structures under load. Structures made using Pultruded Rod Stitched Efficient Unitized Structure (PRSEUS) for damage tolerant, light, and economical airframe construction are being pursued by The Boeing Company and NASA under the Environmentally Responsible Aircraft initiative (ERA). The failure tests of two PRSEUS substructures based on the Boeing Hybrid Wing Body fuselage concept were conducted during third quarter 2011 and second quarter 2015.

One fundamental concern of these tests was determining the effectiveness of the stitched integral stiffeners to inhibit damage progression. By design, severe degradation of load carrying capability should not occur prior to Design Ultimate Load (DUL). While minor damage prior to DUL was anticipated, the integral stitching should not fail since this would allow a stiffener-skin delamination to progress rapidly and alter the transfer of load into the stiffeners. In addition, the stiffeners should not fracture because they are fundamental to structural integrity.

Getting the best information from each AE sensor is a primary consideration because a sparse network of sensors is implemented. Sensitivity to stiffener-contiguous degradation is supported by sensors near the stiffeners, which increases the coverage per sensor via AE waveguide actions. Some sensors are located near potentially critical areas or "critical zones" as identified by numerical analyses.

The approach is compared with the damage progression monitored by other techniques (e.g. ultrasonic C-scan).

Michael R Horne, National Institute of Aerospace, 100 Exploration Way, Hampton VA 23666-6147, U.S.A..
Peter D Juarez, NASA Langley Research Center, Hampton VA 23681, U.S.A.

INTRODUCTION

Composite structures assembled from panels of the PRSEUS concept were mechanically tested for damage tolerance at different scales of complexity [1-6]. The panel construction is fully stiffened using stitched and co-cured stiffening frames and stringers as indicated in Figure 1. The stitched interface is designed to arrest damage propagation.

Two structures monitored for AE during testing are the Pressure Cube and the MultiBay Box (MBB) seen in Figure 2. The Pressure Cube is a portion of the MBB designed to evaluate the pressure rating of the PRSEUS panels. The MBB is a portion of the Boeing Blended Wing Body designed to evaluate the response to flight conditions of various combinations of wing loads and pressurization. Both are part of a wing-body airframe concept assembled with a minimum of fasteners and constructed of large PRSEUS panels. For more details on the construction and other concepts, the reader is urged to investigate the broader PRSEUS literature beyond [1-6].

TEST CONFIGURATIONS AND AE ANALYSES

The AE sensors (piezoelectric, 0.75 inches in diameter by 0.75 inches in height) were bonded onto aluminum adhesive tape applied to the test articles for easy removal. The sensors are connected relatively close to preamp/line drivers to buffer the signal back to the data acquisition system. Each sensor has its own data acquisition channel. Channel identification numbers match sensor identification numbers.

The sensors were attached to the outside of the test articles and primarily co-located with the stiffeners on the inside of the articles [5, 6]. The evidence supporting this approach is discussed in the following section.

For the Pressure Cube and the MBB, a complete coverage of the structure with sensors was difficult. For the MBB some locations were chosen to cover critical areas identified in a nonlinear analysis for loads beyond DUL [3]. The remaining sensors were

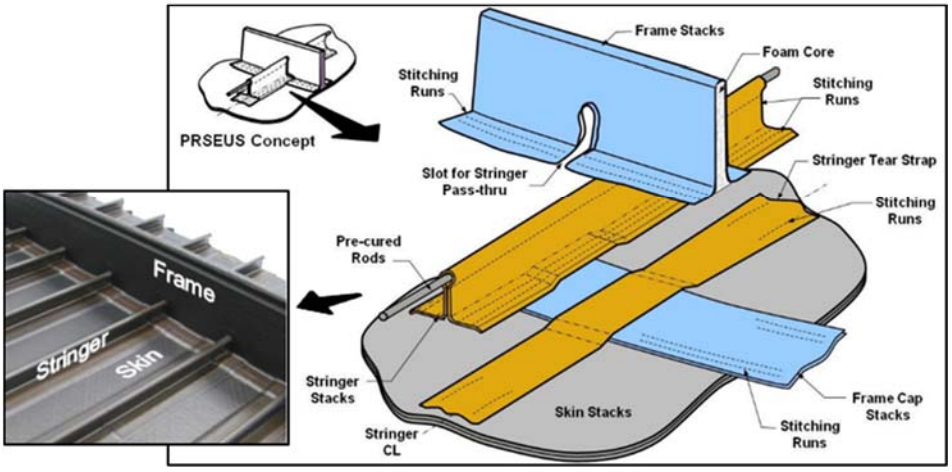

Figure 1. PRSEUS unitized structural concept test panel (inset photo). Derived from [1]

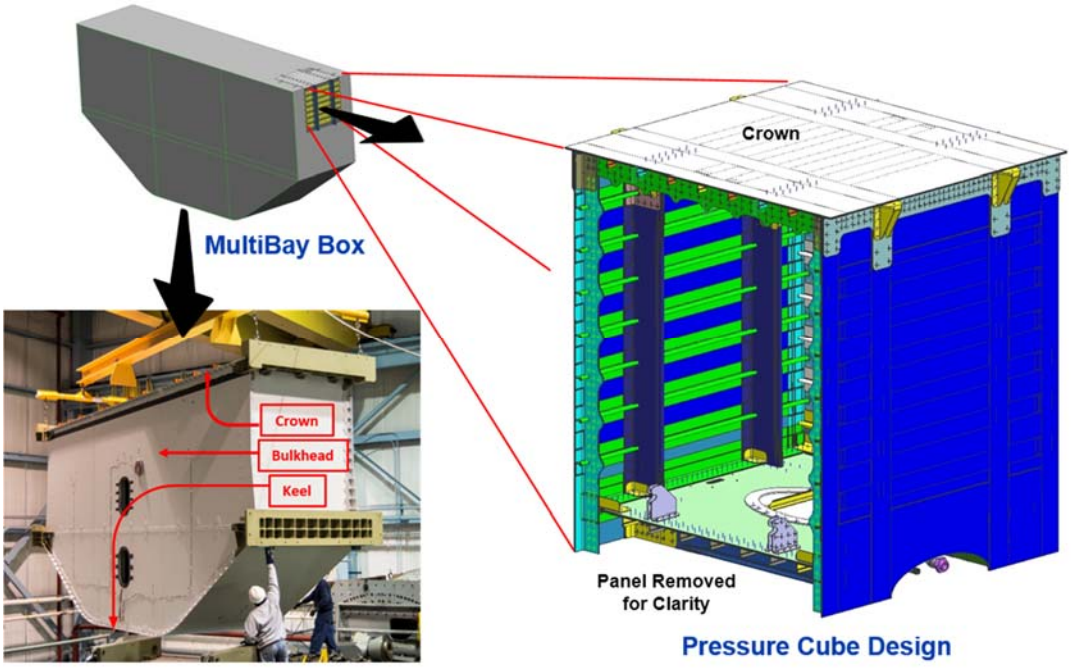

Figure 2. PRSEUS test articles: Pressure cube and MultiBay Box

located near other regions of interest and located outside of areas speckled for optical strain mapping.

Acoustic emission systems collect structure-borne and generated sound, in the ultrasonic frequency band (approx. 50 to 500 kHz). It is generated by dynamic displacements in the picometer range [5]. It is useful to record and measure these ultrasonic emissions because they can be used to locate and track the damage development and evolution that is a precursor to failure. The total electrical energy, generated by an acoustic signal as received by the transducer is proportional to the area under the transducer's voltage^2-time curve, with units of $V^2\mu sec$. A useful presentation of this data is given by plotting the energy in a cumulative manner against time or other appropriate experimental variable.

WAVE PROPAGATION IN PRSEUS STRUCTURES

Wave propagation in a complex structure is subject to reflection, refraction, and diffraction when encountering boundaries, such as changes in microstructure and geometry. To evaluate wave propagation (AE) from damage development in a PRSEUS structure, an experimental investigation was conducted in a PRSEUS panel with approximate dimensions of 4 ft. by 8 ft. It had a frame (see Figure 1) running lengthwise on the centerline and stringers perpendicular to the frame spaced at every six inches. Not included on this panel are end caps (or t-caps). They are another type of stiffener at the edge of a panel used as a flange to attach perpendicular panels. A cap is constructed like a larger stringer without the tubular edge containing a pultruded rod. This similarity

to a stringer also extends to the effect on wave propagation in the skin to which a stringer or cap is attached as an integral part of the lay-up.

Standardized pencil lead breaks (PLB) [5] were used to simulate the stress wave generation of damage development in the material. The step unload and the resultant wideband AE created by a PLB is more of a function of the response of the material and structure, than the application of the load. In plate-like structures, the resultant plate wave propagation can be very similar to that generated by microstructural damage development.

Six series of PLBs were conducted on the smooth side of the panel. The AE sensors were also located on the smooth side. For triggering consistency, a stationary trigger sensor was located at a short fixed distance from the stationary PLB location. A non-stationary sensor captured the wave propagation from three PLBs per location, at increasing distances along lines in strategic directions from the PLB location. Two of the series were conducted on lines perpendicular to, and crossing over, the frame run to evaluate the effects of the acoustic impedance of the frame on wave propagation. One of those lines was in a bay (skin region bounded by stringers and frames) off-center between two stringers: two inches from one and four inches from the other. The other line, collinear with a stringer run, was also to evaluate the waveguide potential of a stringer. Four of the series were conducted on lines perpendicular to the stringers, crossing over three stringer runs, to evaluate acoustic impedance of the stringers on wave propagation. Three of those lines are on the frame run; one along the center of the frame over the foam core ("on center"), one over one of the frame faces (portion of frame stacks perpendicular to the skin, denoted "on side") and one along the centerline of the frame flange ("on flange"). These also helped to evaluate the ability of the frame to act as a waveguide. The fourth line was on the midline between the frame run and the edge of the panel ("In Bay") for evaluation of the acoustic impedance of the stringers without interference from the frame or panel edge. The suggestion that a structural feature acts as a waveguide does not preclude propagation elsewhere in the structure. It is an ability of that feature to propagate sound further with less attenuation than other features.

Figure 3 shows plots of the signal amplitude, that was captured every six and three inches, for the crossing-frame runs (3a) and the crossing-stringer runs (3b), respectively. The captured data from the three PLBs at each location was adjusted to zero dB gain. The plotted values are the mean of the peak amplitudes with one standard deviation

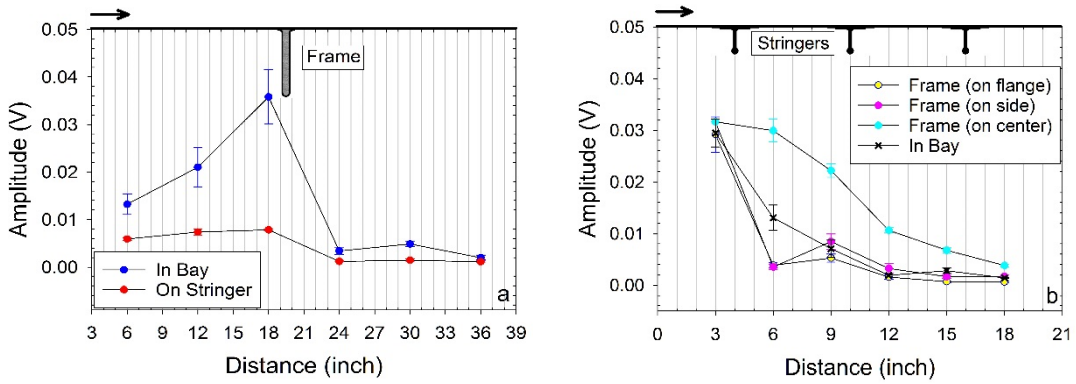

Figure 3. Amplitude of wave propagation (with error bars of one standard deviation): a) perpendicular to frame, and b) perpendicular to stringers

error bars. The black arrows in the upper left corners indicate the wave propagation direction along the skin from PLB location (0 inches). On the upper axis of the plots, schematics of a frame cross-section (3a) and stringer cross-sections (3b) are superimposed to denote where the wave propagation in the skin crosses the frame located at 19.5 inches and the stringers located at 4, 10, and 16 inches.

Frames affect wave amplitudes near the boundaries as indicated by the drop in amplitude as waves propagate across the frame as seen in Figure 3a. The frame also affects skin propagation modes more than the stringer modes. This may be attributed to the fact that the stringer is one continuous structure from panel edge to panel edge. Any guided wave that is supported by the stringer does not encounter changes in the structure as it passes through a keyhole cut in the frame for passage of the stringer. Whereas, because the stiffening structures are infused and co-cured integral with the skin, propagation in the skin encounters stitches and changes in thickness and other geometry where the skin is attached to the frame.

The wave amplitude in the skin (bay) or in a stringer actually increases approaching the frame as seen in Figure 3a. One should note that the sensors are only measuring the amplitudes at the surface and not the full energy flux. Variations such as this may be attributed to behavior such as guided mode transients or constructive interference with reflections, and not an increase in energy flux.

In Figure 3b, the propagation in a bay (black x) is less affected by crossing a stringer than the frame modes crossing the stringer, with one exception. This is a reversal of the behavior in Figure 3a. This may be attributed to the large discontinuities in the frame created by the keyholes cut in the frame for the stringers to pass through. For the skin (bay) propagation, the stringer creates a smaller change in geometry. However, an exception seems to be the "Frame (on center)" propagation that shows a smooth change regardless of the stringers and the least reduction of all the tests in Figure 3b. This may be attributed to guided wave propagation in the frame cap stacks (Figure 1) which do not have stitches in the center and that run continuously without kinks under the frame and intersecting stringers.

It is useful to look at the absolute changes in signal amplitude over distance. The range of cross-stringer reductions (3b) over 15 inches is calculated to be from 18.3 dB (frame: on center) to 33.2 dB (frame: flange). The cross-frame reductions (3a), over a greater distance of 30 inches, are both less at 16.5 dB in the bay and 14.3 dB along the stringer run. This supports the contention that stringers are good waveguides in a PRSEUS structure.

Therefore, in summary, AE sensors may be located on the stringer runs for optimizing sensitivity to critical damage development. The next best location is on the center of the frame run. Locating a sensor in a bay is not suggested because the stiffening structures (stringers and frames) maintain structural integrity and damage in a bay is not likely to become critical until it propagates to a stiffener. In addition, the stiffening structures are more likely to be initiators of damage in long-term fatigue due to their geometric discontinuity creating local stress raisers.

HIGHLIGHTS FROM PRESSURE CUBE TESTS

For the Pressure Cube a series of tests were conducted at increasingly higher pressure: 0.5P (two tests), 1P, 2P, (P = design pressure = 9.2 psi), and then lastly to

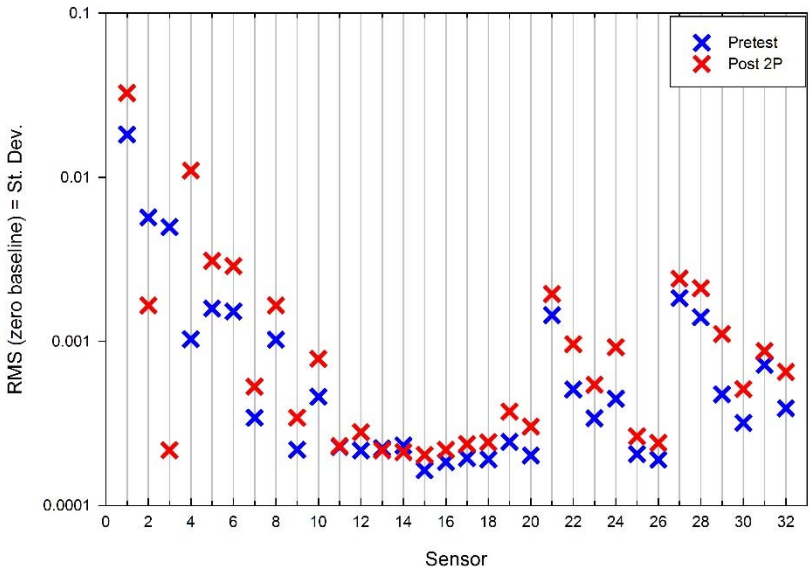

Figure 4 RMS values of signals received at all sensors from PLB at sensor 1

failure. One impact was applied to a particular type of panel called a rib panel on the skin side at an intersection of a t-cap and stringer after the 2P test. During the last test, following that impact, failure occurred at approximately 5P. The blowout of a bulkhead panel was initiated by failures in the impacted rib panel. The failure mode included a metallic frame splice, frame buckling, and integral cap failure all on the side of the panel that included the impact location, and was contiguous to the bulkhead panel.

AE signals from the two 0.5P "checkout" tests were much smaller than events occurring in later tests and only six events occurred in total. Typically, early events such as these are not considered critical damage. During the second 0.5P test only two events occurred. The first event was a damage-AE-like signal and was captured by the sensors on the impacted rib panel, albeit prior to impact. The second event was a damage-AE-like signal captured on the sensors of the blown out bulkhead panel, albeit prior to the failure test. This could indicate a weakness in those two panels. Therefore, the very early AE in a pristine structure may indicate the appropriate regions that should be monitored more closely for structural health evaluation.

Indications of damage were discovered when two series of PLBs were executed: one prior to pressurization ("pre-test") and one after the applied impact ("post-2P") but before the final failure test. The PLBs were conducted approximately an inch away from each sensor in the same consistent manner as noted in the standard and signals collected from all sensors (see discussion in [5]).

For these PLB tests, an indication of the energy collected at each sensor was made by calculating the RMS (root-mean-square) value for each collected waveform. For example, Figure 4 shows, for a PLB at sensor 1, two of the post-2P values are lower than the pre-test values. This reduction is the expected response of distributed damage, all other things being equal. Figure 4 also illustrates the opposite behavior where many of the post-2P (and post-impact) RMS values are larger than the pre-test values. Since

these sensors, as noted previously, are only sensitive to surface displacement, they are not measuring the entire flux of energy flow in the plate. Early distributed damage, if significantly smaller than a wavelength, should tend to attenuate wave propagation. However, with later damage localization and growth, such as delamination, wave propagation encountering these damage structures would be subject to reflection, refraction and diffraction. It is plausible that these behaviors could result in increased energy measured at the surface. In fact, simulations by Leckey and Seebo [7] , Sohn et al [8], and Tian, et al [9] show increased out-of-plane cumulative energy in the area of a delamination for waves propagating along a plate. For these tests, it is suggested that in a damaged state prior to formation of a complete delamination, the existing damage (for example network of matrix cracking) could also begin to induce increased energy measured at the surface. Since the sensors were co-located with stringers (potential damage initiators), it is plausible that these results reflect damage creation in those regions.

Therefore, a comparison was executed to count the number of times a sensor received greater signal RMS during the post 2P series. The sensor cables were disconnected for the impact procedure and the PLBs were not performed in exactly the same location for each series. To account for these effects a parametric study was executed where the differences in signal amplitude had to be greater than a threshold level to count as being different. Varying the threshold over a reasonable range and tabulating the results by panel it was shown that; in general, the count was proportional to the extent of the damage accumulation in the panel. The rib panel that initiated failure and the bulkhead panel that blew off had the highest counts. The crown that had delamination early on was typically third and the other two panels had the lowest counts.

Supporting the energy-trapping scenario are the spectra of the PLB waveforms. Comparison of the spectra of signals from the sensors on the bulkhead panel that did not fail, from before any testing to after the 2P test, showed decreased amplitude across all frequencies. The bulkhead panel that failed showed increased amplitude occurring predominantly in the frequencies below 150 kHz.

One might suggest that PLB tests are not monitoring active damage development. However, as noted previously, the wave propagation is very similar to that created by damage. It is also a mode of wave propagation supported by the structure. Therefore, in some manner, it should be sensitive to changes in the mechanical properties of the

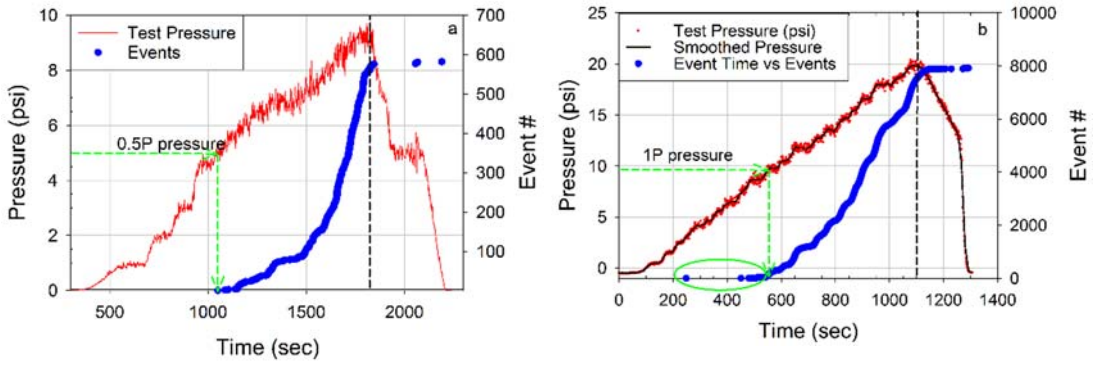

Figure 5. Event plots for Pressure cube tests a) 1P b) 2P (P = 9.2 psi)

structure. Also, a PLB test is a typical tool of an AE practitioner, so if conducted appropriately, could effectively enhance tracking of damage development.

Damage initiation can also be indicated by the timing of AE events relative to the peak load and the previous peak load (see Kaiser Effect [10]). In the plot of pressure and AE events vs. test time for the 1P test seen in Figure 5a, the peak pressure of the previous 0.5P test is denoted by the green dotted line. No AE is occurring prior to this level of pressure, indicating that the 0.5P test did not create any significant damage. However, there are some events occurring during unloading (region to the right of the black dotted line). AE events during unloading typically occur from internal friction of damage surfaces indicating creation of some significant damage during the 1P test. In the plot of pressure and events vs. time for the 2P test seen in Figure 5b, the indication that some significant damage was created during the 1P test is supported further by the AE occurring before the 2P test reaches the 1P pressure level (indicated by the green oval). The larger amount of AE during unloading in the 2P test (relative to the 1P test) indicates even greater extent of damage created during the 2P test. The failure test, not shown here, has an even greater number of AE events prior to reaching the 2P load level than the noted number of events prior to reaching 1P in the 2P test. This indicates an increasing rate of damage development. The Felicity Ratios, which are calculated from the timing of AE events as noted above, [10] for the 1P, 2P, and failure tests are approximately 1.00, 0.76, and 0.65 respectively. The Pressure Cube was a pressure vessel, but the construction is significantly different from a composite overwrapped pressure vessel, so, the failure modes are different. However, for a point of reference, a Felicity Ratio less than 0.95 is a criterion for rejecting composite overwrap pressure vessels during proof testing [11, 12]. Point being, the decreasing Felicity ratio is another indication of the increasing damage development.

To help quantify the meaning of "damage development" the following is a comparison of ultrasonic C-scans and their association with AE that is illustrated in Figure 6. The scans, as seen in Figure 6b, are superimposed over a schematic of the rib

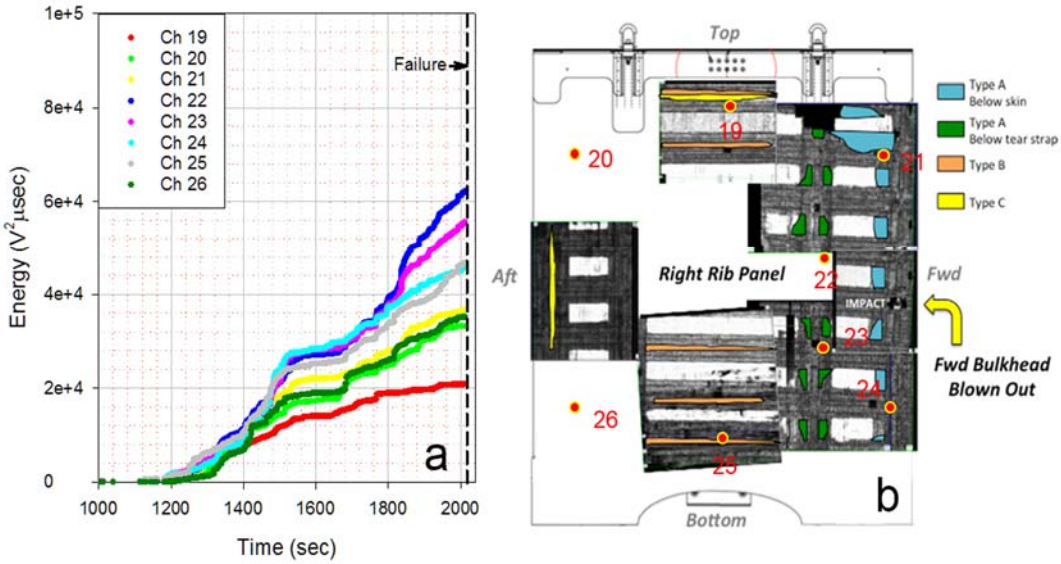

Figure 6. Post-mortem of pressure box impact rib panel. a) AE Cumulative energy for the Failure test. b) Ultrasonic C-scan for the same panel after Failure test.

panel. They are post-mortem scans of the impacted rib panel that initiated the blowout of the contiguous bulkhead panel. The cumulative AE energy, presented in Figure 6a, is of the sensors on the impacted rib panel, during the failure test. The sensor locations are indicated in Figure 6b as the numbered red filled circles.

The C-scans show different types of delaminations [13] denoted by the areas of blue, green, orange and yellow. Frames, stringers and integral caps are indicated by the dark gray stripes. Stringers are horizontal. Frames are vertical at the ¼ and ¾ points widthwise. Integral caps (t-caps) are at the right and left edges of the panel to hold the bulkhead panels. The large majority of delamination acreage is on the right hand side of the panel around the impact and AE sensors 21-25. The right hand edge was the corner of this cube contiguous with the panel that blew out. The right side also contained the metallic frame splice failure at the top near the large blue regions, buckling of the vertical frame under the green delamination acreage, and integral cap failure under the blue acreage. Correlating well with this damage, and indicated in 6a, the sensors with the highest cumulative energy from approximately 1200 seconds until the failure, are sensors 22-25 which are predominately located on the right edge.

Table 1. MBB test matrix with descriptions.

Test Group	CoLTs run #	Test Description and Loads	Test Group	CoLTs run #	Test Description and Loads
Phase I: Checkout	1	Pressure check 2 psi	Phase IV: Checkout	18	4.6 psi (0.5P)
		No test, collected noise		19	31.8 kips (-0.5g)
	2	31.8 kips down-bending (- 0.5g)		20	79.5 kips up-bending (1.25g)
	3	79.5 kips up-bending (1.25g)		21	31.8 kips down-bending + 4.6 psi (-0.5g + 0.5P)
	4	31.8 kips down-bending + 4.6 psi (-0.5g + 0.5P)		22	79.5 kips up-bending + 4.6 psi (1.25g + 0.5P)
	5	79.5 kips up-bending + 4.6 psi (1.25g + 0.5P)	Phase V: DLL	23	63.6 kips down-bending (-1g)
Phase II: DLL	6	12.2 psi (1.33P)		24	63.6 kips down-bending + 9.2 psi (-1g + 1P)
	7	63.6 kips down-bending (-1g)		25	12.2 psi (1.33P)
	8	63.6 kips down + 9.2 psi (-1g + 1P)		26	159 kips up-bending (2.5g)
	9	159 kips up-bending (2.5g)		27	159 kips up-bending + 9.2 psi (2.5g + 1P)
	10	159 kips up-bending + 9.2 psi (2.5g + 1P)	Phase VI: DUL	28	95.4 kips down-bending (-1.5g)
Phase III: DUL	11	95.4 kips down-bending (-1.5g)		29-32	95.4 kips down-bending + 13.8 psi (-1.5g+1.5P): trial 1-4
	12	95.4 kips down-bending + 13.8 psi (-1.5g + 1.5P)		33	95.4 kips down-bending + 13.8 psi (-1.5g+1.5P): success
	13	238.5 kips up-bending (3.75g): trial 1		34	18.4 psi (2P)
	14	238.5 kips up-bending (3.75g): success		35	238.5 kips up-bending (3.75g)
	15	238.5 kips up-bending + 13.8 psi (3.75g + 1.5P)	Phase VII: Combined loads	36-38	Trial 1-3: No AE
	16	18.4 psi (2P): trial 1		39	Trial 4: successful peaks of 262.4 kip and 13.8 psi
	17	18.4 psi (2P): success	Post-sawcut failure	40-42	Trial 1-3: No AE
Impacts		Impacts: Collected AE part-time		43	Trial 4: successful failure at 270 kips

To summarize, aspects of the Pressure Cube AE tests correlate well with damage progression. The PLB analysis, although not AE, does corroborate the extent of the damage, and indicate the potential for expanding the set of useful data without adding much more complexity to the test regimen. The approach to locate sensors on critical structures has resulted in AE data that correlates well with the locations of damage development.

HIGHLIGHTS FROM MULTIBAY BOX TESTS

For the MBB (Figure 2), approximately 40 tests were conducted over 8 phases before and after a series of impacts to the structure were conducted. The target loads and types of loading are noted in Table 1 in chronological order. The structure was cantilevered for the testing and loaded by various combinations of pressurization, up-bending and down-bending. The first, second, and third phases were checkout tests (instrumentation operation), design limit load tests (DLL), and design ultimate load tests (DUL), respectively. The structure was then intentionally impacted in several locations on the bottom plate (keel) and side plates (bulkheads) which created extreme local damage. One impact even penetrated the skin; however, there is no evidence to suggest these impacts initiated any of the damage accumulation that lead to failure of the structure. Therefore, the focus of this discussion will be limited to the top plate (crown) which is illustrated as a schematic drawing in Figure 7. Following the impacts, the first three series were repeated. For the next to last test a schedule of combined loads was conducted where the loads varied independently, but the structure did not fail.

For the final test (denoted as the "post-sawcut failure") the MBB was loaded by up-bending until failure occurred. The frame in the middle of the crown running parallel to the bulkheads was intentionally completely severed on the midline between port and starboard prior to this test. On the schematic in Figure 7, this is represented by the black

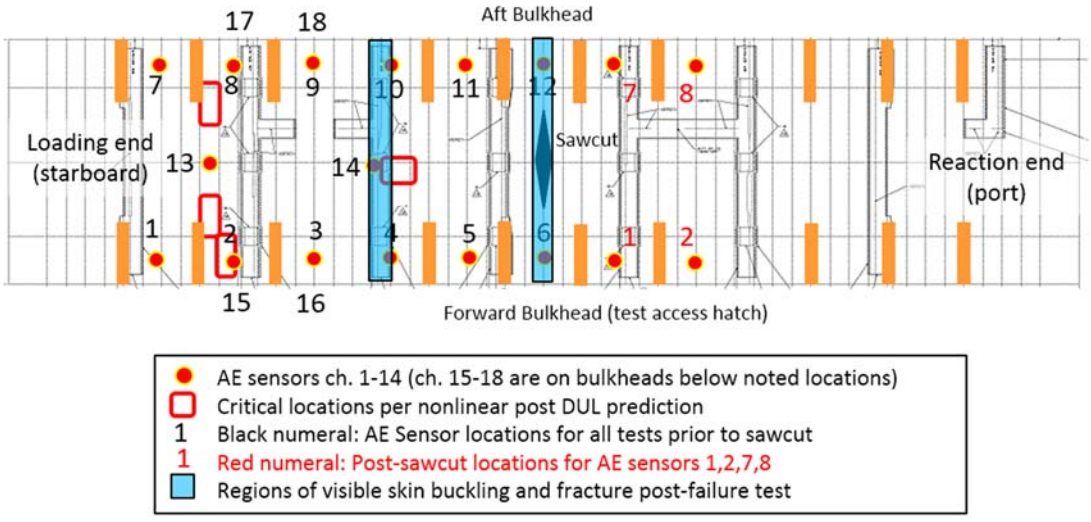

Figure 7. Schematic of MBB crown with AE sensor location, critical areas, and failure regions.

elongated diamond shape between sensors 6 and 12, approximating the shape of the actual sawcut. The fixed or reaction end of the structure is the right hand end of the figure while the loading end is the left. Up-bending denoted in Table 1 is loading out of the paper toward the reader putting the crown predominately in compression lengthwise in the plane of the crown. Down-bending is into the paper, crown is in tension. The location of all the crown AE sensors are indicated by the red filled circles. The red boxes are critical areas identified by a nonlinear prediction of post-DUL behavior[3]. It should be noted that sensors 2, 8, 13, and 14 are located near these critical areas before the post-sawcut test. For the post-sawcut test, sensors 1, 2, 7, and 8 were moved to the reaction (port) side of the saw-cut.

Buckling failure occurred during the last test and extended across the crown in two regions as indicated by the blue strips in Figure 7. The primary buckle extended from the sawcut tips under sensors 6 and 12. The secondary buckle run was under sensors 4, 14, and 10. Extensions of these buckles continued part of the way down the bulkheads. The buckle on the aft bulkhead is a continuation of the secondary buckle extending across sensors 10, 14, and 4. The buckle on the forward bulkhead is the continuation of the primary buckle extending from the sawcut buckle under sensor 6. The offset nature of these indicate some asymmetry in the deformation.

The first three trials for the post-sawcut test identified in Table 1 as tests 40-42 were stopped at loads between 2% and 15% of the previous unprecedented up-bending-only test (test 35 in Phase VI post impact DUL) and no AE was generated. The previous unprecedented up-bending-only test had AE starting at only a few percent of peak load. The fact that two of these trials went higher than that level without generating AE indicates the remaining integrity of the structure. It could be suggested that the sawcut

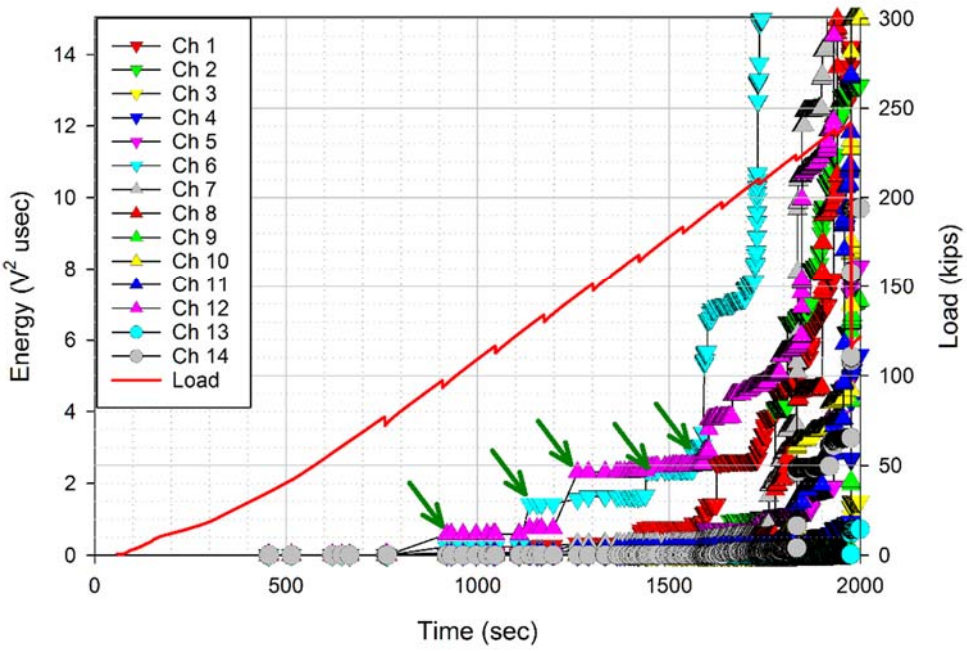

Figure 8. AE Cumulative energy of the MBB crown sensors for the post-sawcut test

actually reduced local stresses similarly to drilling a hole at a cracktip to stop propagation.

In the final trial, highly localized damage started at tips of the diamond shaped sawcut, near sensors 6 and 12, early in the test, around 900 seconds, as indicated in the plot in Figure 8 of cumulative energy vs time. Between approximately 100 and 200 kips (900 to 1600 sec) is an illustration of load shedding. The damage progression switches back and forth from tip to tip as indicated by the alternating energy jumps at sensors 6 and 12 pointed to by the green arrows. The forward bulkhead tip damage (sensor 6) begins to dominate from approximately 200 kip, possibly reducing stresses along the forward bulkhead-crown edge relative to the aft bulkhead-crown edge. This is another indication of some asymmetry in the deformation.

However, the load shedding from sawcut tips as noted above did not begin in a pristine structure. In fact, the behavior is likely predetermined by earlier testing damage. That can be investigated by looking at plots of the total cumulative energy for all tests in a cumulative manner as seen in Figures 9 and 10. Figure 9 contains the first third of the tests ending with the pre-impact DULs. Figure 10 contains the last third of the tests starting with the post-impact DUL load tests. Intervening tests were repeats of earlier tests so little damage accumulation occurred and consequently very little AE was generated.

Starting at the end by looking at Figure 10 there is no obvious indication of when any critical damage occurred near sensors 6 and 12. In fact, sensor 6 is near the top of the range of cumulative energy, sensor 12 is near the bottom, and very little accumulation occurs for most of the tests. Also it should be noted that most of the forward edge sensors (1-6, indicated by down pointing triangle) are in the upper half of

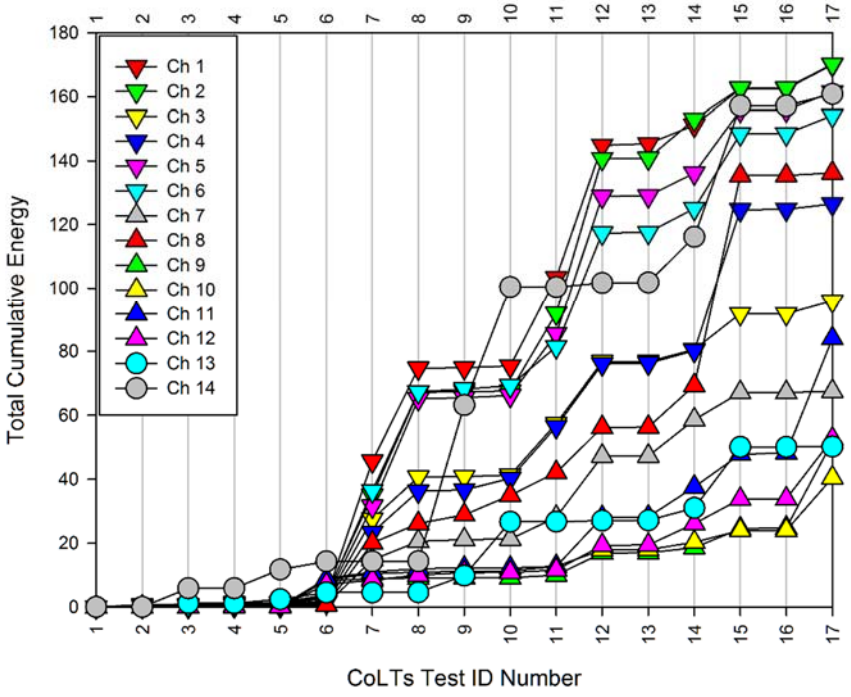

Figure 9. Cumulative AE energy by test for the first seventeen MBB tests.

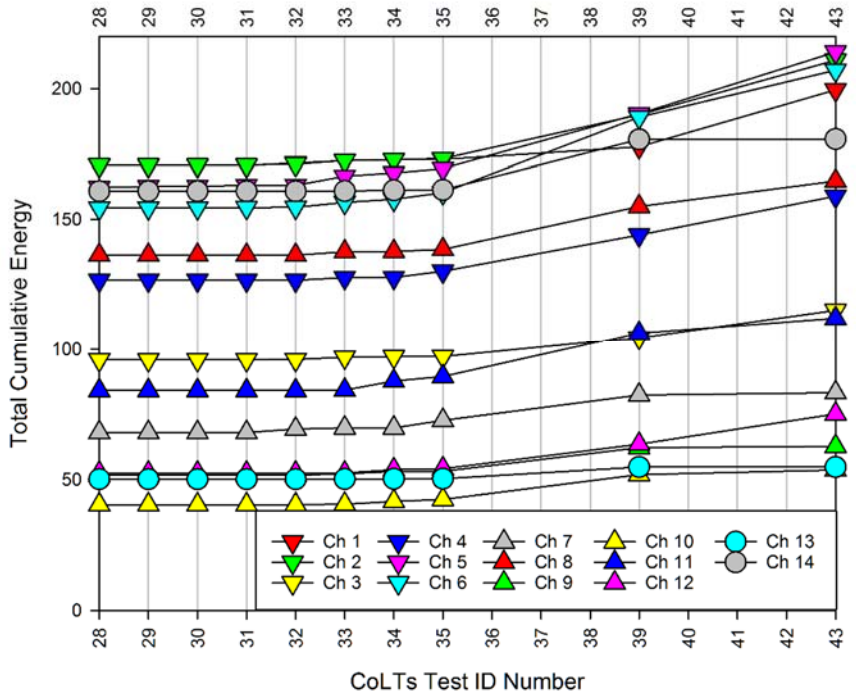

Figure 10. Cumulative AE energy by test for the last sixteen MBB tests.

the energy range while the most of the aft (7-12, indicated by up pointing triangle) are in the lower half. This indicates that the forward edge accumulated more damage. This also supports the concept of load shedding toward the aft side, contributing to the first large increase in sensor 12 in the post-sawcut test. The earlier tests in Figure 9 show significant increases in energy at sensor 6 over sensor 12 during test 7 (first down-bending design limit load), then again in test 8 (down-bending design limit load + pressure). Not much occurs during the subsequent up-bending design limit load tests. This pattern repeats for sensor 6 (and many others) during the ultimate limit load tests: significant increases for the down-bending tests 11 and 12, but not much for the subsequent successful up-bending tests 14 and 15. Test 13, although up-bending, does not exhibit the behavior because it was a trial test that did not reach target loads. Sensor 12 is still near the low end.

Sensors 4, 8, 13 and 14 have distinctly higher increases during test 15, which is up-bending ultimate limit load with pressure. Sensor 4 and sensor 14 are at the forward end and middle, respectively of the future secondary buckle. Sensor 14 is also very near a critical area. It is likely test 15 is the initiation of the weakening contributing to the secondary buckle.

Examining sensor 14 behavior is noteworthy because it is located in a future damage region and in a critical area, and it started to out-increase the others in test 3 (the very first up-bending-only test). It then quickly increased during tests 9 (the next up-bending-only test) and 10 (up-bending + pressure) and eventually moved to near the top of the energy range. Sensor 13, which may be near two critical regions (but not as close as 14 is to its nearest critical area), does not show much increase for the rest of tests and ultimately that region does not appear to have contributed to any failure damage.

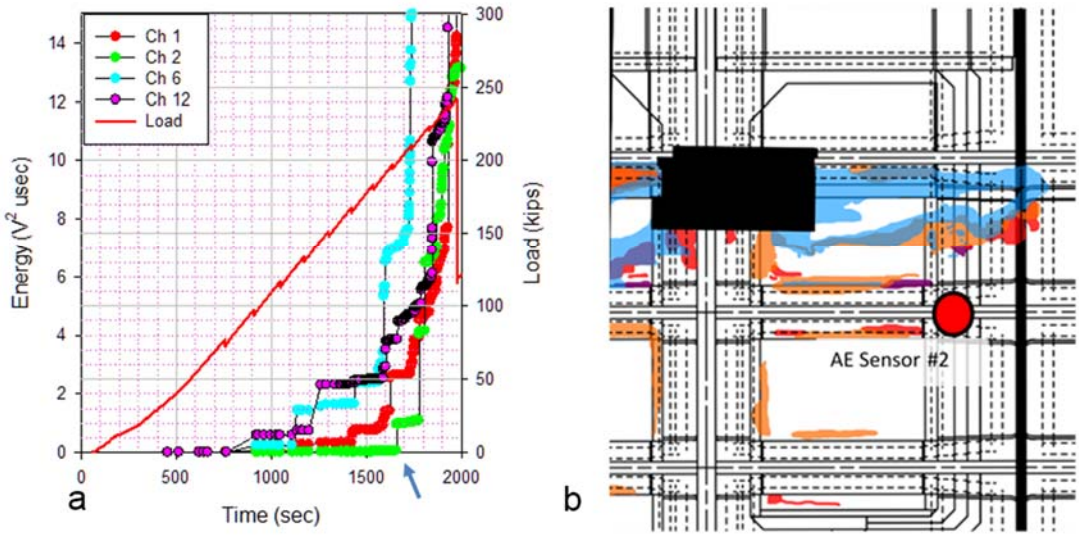

Figure 11. Post-mortem of MBB crown near AE sensor #2. a) AE Cumulative energy for the post-sawcut test. b) Schematic of delaminations discovered by ultrasound after post-sawcut test.

Again, to help quantify the meaning of "damage development" the following is a comparison of ultrasonic C-scans and the AE, illustrated in Figure 11. Seen in Figure 11 is a comparison of the post-mortem schematic of the delaminations found by ultrasonic C-scans of a section of the crown near sensor 2 (11b) and the cumulative energy for the post-sawcut failure test (11a). The different types of delaminations are denoted in 11b by the areas of different colors [14]. The location of AE sensor #2 is denoted as a red dot with black border. The black dashed lines are the stitch lines for the stringers and frames. The solid black lines are denoting changes in geometry such as flange edges, ply drop-offs, or stack faces. In this schematic, the stringers are horizontal at each set of four closely spaced dashed lines. A frame is running vertical on the left side of the schematic under the black region that represents an area that was not scanned. A t-cap runs vertical on the right side of the image under the AE sensor.

Looking at the trace for sensor 2 in 11a there is almost no energy accumulation until approximately 6 minutes before the catastrophic failure. At that time, the first large increase (blue arrow) is likely the beginning of the delamination damage.

To summarize, a beyond-DUL critical area (nr. Sensor 14) which is also included in the secondary buckle of the final up-bending failure, shows higher signal energy accumulation rate over other locations early in the DLL tests. A pattern also exists that shows the down-bending tests created the damage that became critical in the final up-bending failure.

SUMMARY AND CONCLUSIONS

Highlights of results have been presented from "critical zone" locating of AE sensors in a series of large PRSEUS composite structure tests. They indicate that

sensitivity to critical damage is supported by locating sensors near structures where propagating damage becomes critical and where damage is more likely to initiate. Sensitivity is enhanced by locating sensors on features that act like waveguides. In PRSEUS structures, stiffening features are both damage critical and good waveguides.

ACKNOWLEDGEMENTS

The authors would like to acknowledge the support of Ms. Dawn Jegley of NASA Langley for including NDE on the PRSEUS tests.

REFERENCES

1. Velicki, A. and Jegley, D. "PRSEUS Structural Concept Development." AIAA SciTech. 55th AIAA/ASME/ASCE/AHS/SC Structures, Structural Dynamics, and Materials Conference. 13-17 January 2014, National Harbor, Maryland.
2. Vicroy, D.D. Jegley D.C., Cosentino G. "NASA Blended-Wing-Body Research Overview". 67th Annual International Conference on Mass Properties Engineering. Seattle, Washington 2008
3. Velicki, A. "Damage Arresting Composites for Shaped Vehicles," NASA CR-2009-215932, Sept. 2009.
4. Przekop, A, et al. AIAA SciTech. 55th AIAA/ASME/ASCE/AHS/SC Structures, Structural Dynamics, and Materials Conference. 13-17 January 2014, National Harbor, Maryland.
5. Horne, M. R., Madaras, E.I. 2013. "Evaluation of Acoustic Emission SHM of PRSEUS Composite Pressure Cube Tests". NASA Technical Memo: NASA/TM–2013-217993.
6. Horne, M. R., Madaras, E.I. 2016. "Initial Evaluation of Acoustic Emission SHM of PRSEUS Multi-Bay Box Tests". NASA Technical Memo: NASA/TM–2016-218976.
7. C.A.C. Leckey, J. Seebo, Guided wave energy trapping to detect hidden multilayer delamination damage, Rev. Progress Quant. Nondestruct. Eval. 34 (1650) (2015) 1162–1169.
8. H. Sohn, D. Dutta, H. Yang, M. Park, M. DeSimio, S. Olson, E. Swensen Delamination detection in composites through guided wave field image processing, Compos. Sci. Technol. 71 (2011) 1250–1256.
9. Z. Tian, L. Yu, C. Leckey, Delamination detection and quantification on laminated composite structures with lamb waves and wavenumber analysis, J. Intell. Mater. Syst. Struct. (2014). 1045389X14557506.
10. Pollock AA and J.C.Spanner,Sr. 2005. "Chapter 2 Part 1 Fundamentals of Acoustic Emission Testing" in Nondestructive Testing Handbook Third Edition Vol. 6 Acoustic Emission Testing. RK Miller and E vK Hill, tech eds. PO Moore, ed. American Society of Nondestructive Testing. 2005 p 38
11. "Standard Practice for Acoustic Emission Examination of Fiberglass Reinforced Plastic Resin (FRP) Tanks/Vessels". ASTM E1067/ E1067M-11. Committee E07. American Society for Testing and Materials. 2011. p. 15
12. "Fiber Reinforced Plastic Pressure Vessels." in ASME Boiler and Pressure Vessel Code Section X Article RT-6. American Society of Mechanical Engineers. p. 90. 2015.
13. Johnston, P. Ultrasonic Nondestructive Evaluation of PRSEUS Pressure Cube Article in Support of Load Test to Failure. NASA/TM-2013-217799. 2013
14. Johnston, P. and P. Juarez. Ultrasonic Nondestructive Evaluation of Pultruded Rod Stitched Efficient Unitized Structure (PRSEUS) During Large-Scale Load Testing and Rod Push-Out Testing. NASA/TM-2016-218978. 2016.